# Tunable stochastic resonance based on the optimization of centrifugal distance for rotation-induced energy harvesting

# \Tunable Stochastic Resonance Based on the Optimization of Centrifugal Distance for Rotation-Induced Energy Harvesting


## Abstract

Energy harvesting from rotating systems has been developed into an important topic as a promising solution for realizing the powering applications of tire monitoring systems. Because of relatively narrow bandwidth of the efficiently operating response, this paper proposes a principle for optimizing the centrifugal distance for tuning frequency matching between stochastic resonance and the external rotation environments. It can minimize the negative effect of a low energy orbit owing to the optimally stabilized stochastic resonance, particularly over the low frequency range before high energy orbit oscillation. The centrifugal force caused by the behavior of rotation acting on the tip mass of the cantilever changes the equivalent stiffness of the cantilever and thus can tune the variation in the Kramers escape rate. Through the match-able relationship of a non-linear bitable system between the Kramers rate and the external rotation frequency, the expression of the optimally centrifugal distance can be solved by theoretical derivation and numerical analysis. The results of simulations and laboratory experiments simultaneously demonstrate that the centrifugal distance is tuned to be the optimal 6.45 cm as theoretically analyzed, and the effective bandwidth of energy harvesting can be stabilized from 30 rad/s to 50 rad/s. While its maximum root mean square (RMS) voltage can reach the value of 1.23 V corresponding to a harvesting average power of 45.55 μW, owing to the high matching relationship between stochastic resonance and external rotation frequencies. Thus, by the theoretical optimization of centrifugal distance, the frequency of stochastic resonance can be tuned for matching the externally rotating environments, and further improving the operating performance of rotating-induced energy harvesting.


Keywords—Rotation, Tunable stochastic resonance, Optimized centrifugal distance, Energy harvesting

## 1. INTRODUCTION

In daily driving, proper tire pressure can not only prolong the service life of tires, but also improve ride comfort; more importantly, it can reduce traffic accidents caused by failure with respect to tire pressure. The tire pressure monitoring system (TPMS) is an electromechanical system designed to monitor the air pressure inside inflated tires of automobiles, aircraft chassis, overhead cranes, forklifts and other vehicles. However, most batteries in tire pressure sensors are button batteries [1], which are complex and expensive to replace; meanwhile, they are liable to cause significant pollution [2]. On this basis, state-of-the-art intelligent tire systems require more self-powered multi-sensing integration embedded sensors than battery-powered TPMS sensors causing the higher power requirements [3–5]. To realize such a concept, many researchers have proposed a type of sensor that can power itself without additional consumption by utilizing the conversion of vibrational energy [6–9]. It can effectively convert energy harvested from the surrounding environment into electrical power, which drives low-power electronic equipment to operate normally. Among them, piezoelectric vibration energy harvesters [10] have become one of the best means to convert vibration energy from the environment because of their particular structure, weather-free nature, and ease of miniaturization. Most piezoelectric vibration energy harvesters use cantilever beams [11, 12] to construct a linear system; however, they exhibit poor harvesting performance owing to their narrow operational bandwidth. To address this deficiency, researchers have found that the coupling between the excitation and resonator

can be greatly broadened by using a nonlinear system to improve the capability of vibration-based energy harvesting [13–15]. Nevertheless, because of the co-existence of unstable and low-energy orbits for nonlinear systems, another approach is proposed to enhance the stability of high level oscillations over the broadest possible range, particularly over the lower frequency regions, where it is much more difficult to activate high-energy orbit oscillations by introducing other nonlinear effects [16].

Stochastic resonance is a phenomenon in which noise is added to a weak periodic signal to significantly amplify the output response within a certain probability. It has been used in signal detection [17], fault diagnosis [18], image processing [19], and biological neural analysis [20]. Originally, the frequency of stochastic resonance was mainly determined based on Kramers escape rate theory [21]. Although the theory was then specifically elaborated by McNamara and Hänggi et al. [22, 23] to expand its application possibilities in bistable systems, the non-tunable characteristics between the escape rate of a particle and the external periodic excitation, limits its further development on the application to energy harvesting by employing the nonlinear phenomenon of stochastic resonance.

In the field of energy harvesting, the feasibility of activating stochastic resonance has been theoretically and numerically investigated to enhance energy harvesting ability [24, 25]. An experimental validation study realized the one-degree-of-freedom of stochastic resonance based on the constant Kramer escape rate using a bistable cantilever harvester [26]. Moreover, Leng et al. established the discriminant function of stochastic resonance of the Duffing oscillator, and by adjusting the generalized parameters elaborated the general discipline for the occurrence of stochastic resonance under different conditions of noise intensity and signal frequency [27]. Nevertheless, different from one-degree-of-freedom vibrating environments, externally periodic force is manually added, thus consuming extra energy, and the rotation system can be autonomously self-excited from a combination of gravitational effects and rotation behavior, providing the necessary excitation conditions for the occurrence of stochastic resonance [28]. Meanwhile, it has been revealed that the appearance of stochastic resonance can be validated and even maintained under varying rotation frequencies by adjusting the physically parameters rather than by an exact optimization principle [29–31]. Although Kim et al. revealed that a rotating harvester with a symmetric potential function generates power higher than that with asymmetric potential wells [32], the stochastic resonance can be self-tuned for a wider bandwidth by considering the centrifugal stiffness effect; however, the remaining issue of exploring the theoretically optimal relationship between stochastic resonance and external rotation frequencies should be solved for facilitating its potential applicability.

Furthermore, a rotational energy harvester using frequency up-conversion and bistability was proposed for stabilizing and improving the output over a wide bandwidth at low frequencies without considering the rotationally centrifugal effect [33]. An electromagnetic energy harvester was considered for low frequency and irregular vibration, further the triboelectric nanogenerator was developed based on the dynamic behavior of the system combing with adaptive-anastomotic barricades for rotational energy harvesting [34, 35]. In addition, a rotationally piezoelectric beam assembled bistable energy harvester was presented for demonstrating the performances at low or high rotational frequencies in the presence of the centrifugal stiffening or softening effects [36, 37]. A tristable or quad-stable cantilever energy harvester was investigated for enhancing the efficiency of energy harvesting in low-frequency rotational environment [38–40]. Nevertheless, the random noise excitation which are usually accompanied during the rotating from environments in practice, cannot be neglected due to its large amount of vibrational energy over a broadband frequency existed, thus potentially activating the different kind of oscillating phenomenon resulting from the complexity of nonlinear vibration. On this basis, stochastic resonance which not only can harvest energy generating from rotationally periodic force of harmonic gravity, but can simultaneously harvest energy from externally vibrating environment of noise excitation. Moreover, after the centrifugal effect is added, the tunable characteristic has the ability to potentially harvest energy over a wider frequency range of rotating environments than a constant rotating frequency under non-tunable stochastic resonance.

In response to the limitations of the state-of-the-art, this paper proposes a principle of optimizing the centrifugal distance for a bistable system, for tuning frequency matching between stochastic resonance and the external rotation environment. Through the solvable match relationship of a non-linear bistable system between the Kramers escape rate and the external rotation frequency, the optimal centrifugal distance can be determined by the theoretical solution as well as numerical analysis. The simulation results demonstrated that the centrifugal distance is tuned to be the optimal 6.45 cm as theoretically analyzed, the effective bandwidth of energy harvesting can be stabilized from 30 rad/s to 50 rad/s, with the maximum average power of 45.55 μW, and the experimental results are in good agreement with the numerical simulation, which reveals that the theoretically tunable principle of stochastic resonance based on the optimization of centrifugal distance can effectively improve the performance of rotation-induced energy harvesting.

## 2. STIFFNESS TUNABLE DYNAMIC MODELLING

Figure 1(a) shows a schematic diagram of the mechanical structure of the energy harvester mounted from the rotating center of *o*. It comprises a rectangular cantilever beam with a piezoelectric film attached to the root of the beam, and two magnets with the same polarity located at the free end of the cantilever and the frame of the energy harvester. When the energy harvester revolves around the *x* axis with a rotation frequency of $\omega$, if the appropriate value of the distance *d'* between the magnets is adjusted, under the action of the repulsive force $F_N$ corresponding to its tangential component of $F_T$ between the magnets and the restoring force $kx_r$ of the cantilever beam, the end magnet of the cantilever can reflect bistable characteristics by the transition movement between two potential wells. As shown in figure 1(b), the conceptual design of the assembled setup is convenient for adjusting the distance from fixed base of cantilever to rotation center. The displacement sensors were located perpendicularly to the cantilever beam to measure the dynamic responses of the energy harvester.

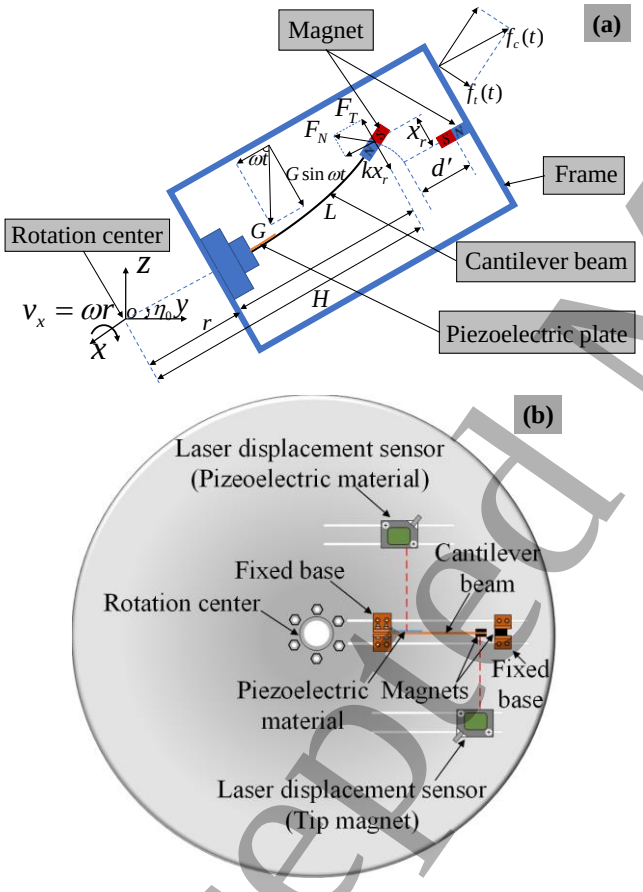


**Figure 1.** (a) Schematic of rotation-induced energy harvesting model owing to centrifugal force effect and (b) conceptual diagram of the assembled setup.

A typical Duffing dynamic equation of a bistable system under harmonic excitation [41] is expressed as

$$m\ddot{x}_r + c\dot{x}_r - a_0' x_r + b' x_r^{\,3} = \xi \sin\left(\omega t + \eta_0\right), \qquad (1)$$

where $x_r$ is the tangentially instantaneous displacement of the cantilever at the tip position, *m* is the magnet mass, and *c* is the viscous damping coefficient, including mechanical and electrical elements. The symbol $a_0'>0$ defines the linear coefficient term resulting from the lateral stiffness of the cantilever beam and the repulsive effect between two magnets with the same polarity. The symbol $b>0$ is the nonlinear coefficient term of the magnetic repulsion, and a harmonic force $\xi\sin(\omega t+\eta_0)$ is added as the external excitation emerging as a vertical component of the load on the cantilever beam with a rotating frequency $\omega$ from an initial angle $\eta_0$ defined between the central axis of the beam and the horizontal direction.

The Duffing dynamic equation in a rotating environment is established based on the Lagrange theorem [28] to satisfy the occurrence condition of stochastic resonance, as governed by equation (2).

$$m\ddot{x}_r + c\dot{x}_r - a_0' x_r + b' x_r^{\,3} = \left(G + N(t)\right)\sin\left(\omega t + \eta_0\right), \qquad (2)$$

where the harmonic force is treated as $G+N(t)=\xi$, *G* represents the gravity of the tip magnet, $N(t)=\sqrt{(2D)}\varsigma(t)$ is the external noise excitation, in which *D* denotes the intensity of the noise $\varsigma(t)$, which is a zero-mean, one-variance Gaussian white noise, and $(G+N(t))\sin(\omega t+\eta_0)$ is noted to be the harmonic function when the external noise excitation is added. Considering the effect of the magnetic repulsion of $F_T$, the expressions of the linear and nonlinear coefficients are detailed as $a_0'=\varphi v^2(9M_{cx}M_{fx}-12M_{cy}M_{fy})/4\pi d'^5-k$, and $b'=\varphi v^2(75M_{cx}M_{fx}-90M_{cy}M_{fy})/8\pi d'^7$, respectively, where *k* is the stiffness of the cantilever beam, *v* and $\varphi$ are the volume of the magnets and the permeability of free space, respectively. $M_f=(M_{fx},M_{fy})$ and $M_c=(M_{cx},M_{cy})$ are the magnetization strength amplitudes of the magnets attached to the frame and the magnetic tip mass, respectively.

While the energy harvester rotates in the clockwise direction, as shown in figure 1, the tangential component generated from the centrifugal force of the tip mass $f_c(t)$ is given as [42, 43]

$$f_t(t) = \frac{3m\omega^2(L+r)}{2L} x_r(t), \qquad (3)$$

where *r* is the distance from the root of the beam to the center axis of rotation, *L* is the length of the beam, and by introducing the tangentially centrifugal effect on the external excitations, and motion for the piezoelectric unit directly powering a resistive load as a current source according for Kirchhoff laws, the coupled dynamic equation of the rotating bistable energy harvester adopted to nonlinear oscillation is expressed as [44–48]

$$\begin{aligned} &m\ddot{x}_r + c\dot{x}_r - a_0' x_r + b' x_r^{\,3} \\ &= -f_t(t) + (G + N(t))\sin\left(\omega t + \eta_0\right) - \theta_p CV\,, \end{aligned} \qquad (4)$$

$$\theta_p C\dot{x}_r = \frac{V}{R} + C\dot{V}\,, \tag{5}$$

where $\theta_p$ represents electromechanical coupling coefficient, $C$ denotes the capacitance of the piezoelectric unit, and $V$ is the voltage generated by the piezoelectric unit. $R = R_i + R_l$, where $R_i$ and $R_l$ are the internal and external load resistances, respectively. To explain how the piezoelectric unit operates in the mechanical system, equation (5) can be expressed as

$$\boldsymbol{V} = \frac{\theta_p s}{s + 1/RC}\boldsymbol{X}\,, \tag{6}$$

where $s$ is the Laplace transform, $\boldsymbol{V}$ and $\boldsymbol{X}$ are the Laplace transforms of $V$ and $x_r$. It is assumed that the higher-order harmonics are negligible, and the steady state solution of equations (7a) and (7b) can be modelled as

$$x_r = a_1 \sin\omega t + b_1 \cos\omega t\,, \tag{7a}$$

and

$$V = a_2 \sin\omega t + b_2 \cos\omega t\,. \tag{7b}$$

Then

$$\dot{x}_r = a_1\omega\cos\omega t - b_1\omega\sin\omega t\,, \tag{8a}$$

$$\dot{V} = a_2\omega\cos\omega t - b_2\omega\sin\omega t\,, \tag{8b}$$

and

$$\ddot{x}_r = -a_1\omega^2\sin\omega t - b_1\omega^2\cos\omega t\,. \tag{8c}$$

Substituting equations (7) and (8) into equation (4), collecting coefficients with the same structure yields

$$b_1 Q_a + Q_b a_1 - \theta_p C b_2 = G\,, \tag{9a}$$

and

$$a_1 Q_a - Q_b b_1 - \theta_p C a_2 = 0\,, \tag{9b}$$

where

$$Q_a = \frac{3b'}{4}x_r^{\,2} - m\omega^2 - a'\,, \tag{10a}$$

$$Q_b = c\omega\,. \tag{10b}$$

Similarly, substituting the steady-state solutions of equations (7) and (8) into equation (5), it is given that

$$a_2 = \frac{\theta_p C\omega\left(-b_1/R + C\omega a_1\right)}{1/R^2 + C^2\omega^2}\,, \tag{11a}$$

and

$$b_2 = \frac{\theta_p C\omega\left(a_1/R + C\omega b_1\right)}{1/R^2 + C^2\omega^2}\,, \tag{11b}$$

By squaring equations (9a) and (9b) while adding the left and right terms, respectively, it can be obtained as

$$Q_a x_r^{\,2} + Q_b x_r^{\,2} + \left(\theta_p C\right)^2 V^2 - 2\theta_p C a_2\left(Q_a a_1 - Q_b b_1\right) - 2\theta_p C b_2\left(Q_a b_1 - Q_b a_1\right) = G^2\,, \tag{12a}$$

where

$$x_r^{\,2} = a_1^2 + b_1^2\,, \tag{12b}$$

$$V^2 = a_2^2 + b_2^2 = \frac{\left(\theta_p\omega x_r\right)^2}{\omega^2 + 1/R^2C^2}\,. \tag{12c}$$

Moreover, equation (12c) can be rewritten as

$$V = \frac{\theta_p}{\sqrt{1 + 1/\omega^2R^2C^2}}x_r\,. \tag{13}$$

Therefore, the voltage produced across the external load resistance $R_l$ can be written as follows:

$$V_l = \frac{R_l}{R_i + R_l}\frac{\theta_p}{\sqrt{1 + 1/\omega^2(R_i + R_l)^2C^2}}x_r\,, \tag{14}$$

and the harvested power via the external road resistance is arranged as

$$P_l = \frac{R_l\theta_p^{\,2}x_r^{\,2}}{\left(R_i + R_l\right)^2 + 1/\omega^2C^2}\,, \tag{15}$$

where $R_i$ can be calculated by theoretically matching the impedance $1/j\omega C$ of the equivalent capacitance of the piezoelectric model. By substituting equation (3) into equation (4) and rearranging the linear term coefficients, the stiffness tunable dynamic equation of the system is obtained as follows:

$$\begin{aligned} m\ddot{x}_r + c\dot{x}_r + \left(a_0' - \frac{3\mathrm{m}\omega^2\left(L + r\right)}{2L}\right)x_r + b'x_r^{\,3}\,, \\ = \left(G + N(t)\right)\sin\left(\omega t + \eta_0\right) - \theta_p CV \end{aligned} \tag{16}$$

where

$$a_0 = a_0' - \frac{3M\omega^2\left(L + r\right)}{2L}\,. \tag{17}$$

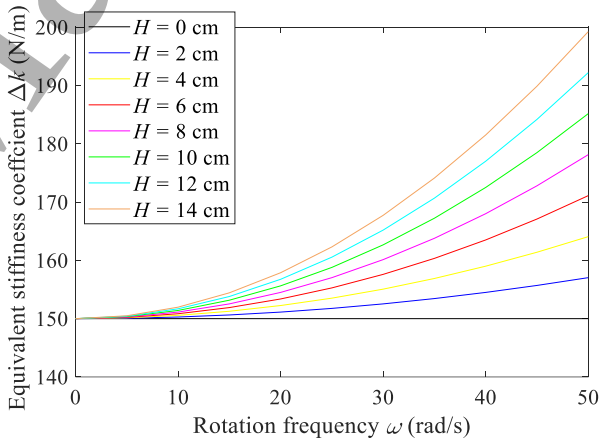


**Figure 2.** Equivalent stiffness coefficient $\Delta k$ as a function of $\omega$ under different centrifugal distances.

Hence, the equivalent effect of the centrifugal force on the stiffness of the cantilever beam is given as [49]

$$\Delta k = k + \frac{3M\omega^2 H}{2L}\,, \tag{18}$$

where the centrifugal distance of $H$ is defined by the distance of $r$ from the root of the beam to the center axis of rotation, plus the length of the beam $L$. By setting the parameter values $k$=150 N/m, $m$=0.0075 kg and $L$=0.08 m, figure 2 shows the variation trends of equivalent stiffness of the cantilever beam $\Delta k$ with respect to the rotation

frequency $\omega$ at different centrifugal distances from zero to 14 cm. It can be seen that the equivalent coefficient of the cantilever beam exhibits stiffer properties with an increase in the rotation frequency at different centrifugal distances.

## 3. OPTIMIZATION OF TUNABLE STOCHASTIC RESONANCE

When the amplitude of the periodic excitation is too weak to activate the transition of particle between two potential wells, the cantilever can only fluctuate within one potential well. It is assumed that the cantilever can jump across the potential barrier for the inter-well motion after the external noise input is added to the periodic excitation, and the transition is synchronized with the inclination of the potential well. The average waiting time $T_F$ of the transition is 1/2 of the periodic excitation period $T_B$, which can be defined using equation (19).

$$T_B = 2T_F\,, \tag{19}$$

where the frequency of the particle transition within one potential well is determined based on Kramers rate theory. Using the Kramers escape rate $\gamma_k$, the one-time period of stochastic resonance is derived as $T_B=2/\gamma_k$. The escape rate $\gamma_k$ [23] within one potential well is written as

$$\gamma_k = \frac{\sqrt{2}a_0}{2\pi c}\exp(-\frac{a_0^{\,2}}{4b'D})\,,\ \text{(unit: Hz)}. \tag{20}$$

Therefore, the tunable expression of stochastic resonance is given as equation (21), it is indicates that the all coefficients of linear, equivalently nonlinear, the viscous damping, and intensity of the noise are related to the probability of stochastic resonance for enhancing the inter-well oscillation.

$$\gamma = \frac{\sqrt{2}a_0}{2c}\exp\left(-\frac{a_0^{\,2}}{4b'D}\right),\ \text{(unit: rad/s)}. \tag{21}$$

According to equations (17) and (21), the frequency of stochastic resonance is tunable with the variation of the rotation frequency of $\omega$, which is optimizable by the definition relationships of $\gamma=\omega$ and $\gamma'=1$, to ensure a good frequency consistency between the stochastic resonance and the externally harmonic rotation excitation. The equation (22) can be obtained by substituting the equation (21) into the expression of $\gamma=\omega$, by substituting the equation (17) into equation (21), differentiating it with respect to $\omega$, and combining with the relationship of $\gamma'=1$, equation (23) is derived and re-arranged as

$$\gamma = \frac{\sqrt{2}a_0}{2c}\exp\left(-\frac{a_0^{\,2}}{4b'D}\right) = \omega\,, \tag{22}$$

$$\gamma' = (\frac{3\sqrt{2}M\omega H}{2Lc})\left\{\frac{a_0^{\,2}-2b'D}{2b'D}\exp\left(-\frac{a_0^{\,2}}{4b'D}\right)\right\} = 1, \tag{23}$$

then, equation (22) can be re-arranged into

$$\exp\left(-\frac{a_0^{\,2}}{4b'D}\right) = \frac{2c\omega}{\sqrt{2}a_0}\,, \tag{24}$$

substituting equation (24) into equation (23) derives

$$\gamma' = (\frac{3M\omega H}{L})\left\{\frac{a_0^{\,2}-2b'D}{2b'D}\frac{\omega}{a_0}\right\} = 1, \tag{25}$$

and it can be re-governed as follows:

$$3M\omega^2 H(a_0^{\,2}-2b'D) - 2a_0 b'LD = 0\,. \tag{26}$$

Assuming $\lambda=\omega^2 H$ and substituting equation (17) into equation (26), a cubic equation with respect to $\lambda$ can be expressed as

$$\frac{27M^3}{4L^2}\lambda^3 - \frac{9M^2 a_0'}{L}\lambda^2 + 3M\lambda(a_0'^2 - b'D) - 2a_0' b'LD = 0\,. \tag{27}$$

Based on the antecedent calculation of the numerical validation, the solution with the physical meaning of equation (27) is retained as

$$\lambda = \psi L/9\,, \tag{28}$$

where,

$$\psi = \frac{4a_0'}{M} - \frac{(1+\sqrt{3}i)(-324a_0'^2 - 972b''D)}{162\times 2^{2/3}M\sigma} - \frac{(1-\sqrt{3}i)\sigma}{2^{1/3}M}\,, \tag{29}$$

and

$$\sigma = \left(\begin{matrix}-2a_0'^3 + 45a_0'b'D \\ +3\sqrt{3}\sqrt{-8a_0'^4 b'D + 71a_0'^2 b'^2 D^2 - 4b'^3 D^3}\end{matrix}\right)^{1/3}. \tag{30}$$

By substituting equation (17), $\lambda=\omega^2 H$ and equation (28) into equation (22), respectively, the frequency of the tangent point of $\omega_T$ for the matching between frequencies of stochastic resonance and harmonic rotation can be solved as

$$\omega_T = \frac{\sqrt{2}(6a_0' - M\psi)}{12c}\exp\left(-\frac{(6a_0' - M\psi)^2}{144b'D}\right). \tag{31}$$

By transforming the relationship between $\lambda=\omega^2 H$ and equation (28), the centrifugal distance can be expressed as

$$H = \frac{\lambda}{\omega^2} = \frac{\psi L}{9\omega^2}\,. \tag{32}$$

Substituting the expression of $\omega_T$ based on equation (31) into equation (32) yields the optimal expression of centrifugal distance as

$$H_o = \psi L \Bigg/ \left(\frac{(6a_0' - M\psi)^2}{8c^2}\exp\left(-\frac{(6a_0' - M\psi)^2}{72b'D}\right)\right). \tag{33}$$

The relationship of $\gamma=\omega$ is the precondition which is defined with the purpose for the matching of tunable stochastic resonance and external rotation frequency, meanwhile the combination relationship of $\gamma'=1$ by a mathematical assignment can make the derivation and obtaining of cubic equation (27) become possible. Nevertheless, whether the optimal centrifugal distance can be finally solved and theoretically defined, the existing of solution by $\lambda=\psi L/9$ which can reveal the frequency of

tangent point of $\omega_T$ for the matching between frequencies of tunable stochastic resonance and harmonic rotation frequency. Therefore, the expression of the tangent point of $\omega_T$ derived can be treated as a core mathematical index for investigating the improved probability of stochastic resonance over a certain frequency range around the tangent point of $\omega_T$. As for the range definition by the specifically theoretical equation would be an extremely interesting and challenge further work, because the probability for the occurring of stochastic resonance is particularly different from the traditionally definite linear or nonlinear resonances.

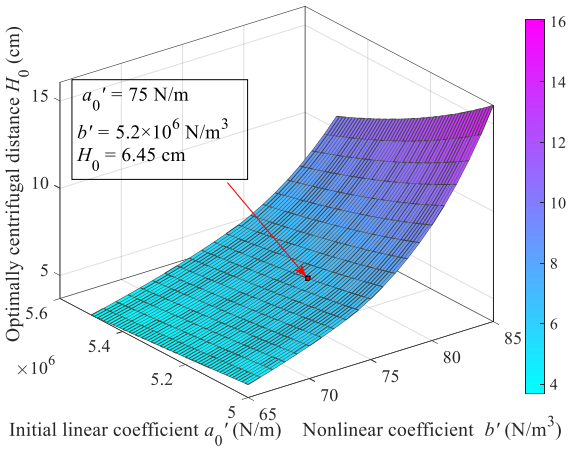


**Figure 3.** Diagram of optimally centrifugal distance $H_0$ versus the variation of the initial linear coefficient $a_0'$ and the nonlinear coefficient $b'$.

Based on the optimal equation of centrifugal distance, the optimally centrifugal distance gradually increases with a decrease in the linear coefficient $a_0'$ and an increase in the nonlinear coefficient $b'$. The physical parameters of the bistable system were determined as $a_0'$=75 N/m, $b'$=5.2×10$^6$ N/m$^3$, $c$=0.251 N/m/s, and the intensity of the white Gaussian noise $D$=1.22×10$^{-4}$ N. It can be clarified that the optimally centrifugal distance is found to be 6.45 cm corresponding to that of the specifically parametric condition, as shown in figure 3.

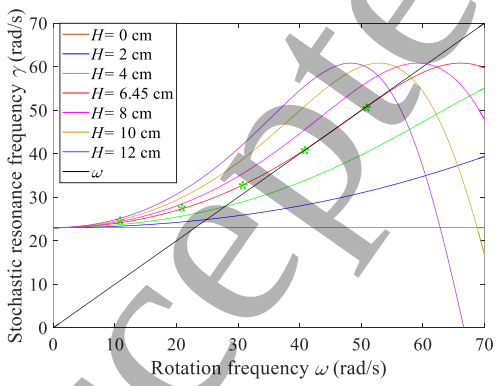


**Figure 4.** Matching investigation of stochastic resonance and rotation frequencies over different centrifugal distances of 0 cm–12 cm.

With the purpose of verifying the frequency consistency between the stochastic resonance and externally harmonic rotation excitation, its tunable curves over centrifugal distances of 0 cm, 2 cm, 4 cm, 6.45 cm, 8 cm, 10 cm and 12 cm are shown in figure 4. It can be interpreted that the curve of tunable stochastic resonance only at a centrifugal distance of 6.45 cm has a good matching with the harmonic rotation frequency, which agrees well with the calculated result of the optimally centrifugal distance, as shown in figure 3, based on equation (33).

## 4. SIMULATION RESULT

All numerical simulations are carried out under the software environment of MATLAB by employing Runge-Kutta algorithm. To verify that the optimized centrifugal distance can significantly broaden the operational frequency range of the stochastic resonance before the oscillation of the high-energy orbit, the boundary frequency between the stochastic resonance and high-energy orbit should be confirmed in advance under the optimized centrifugal distance of 6.45 cm.

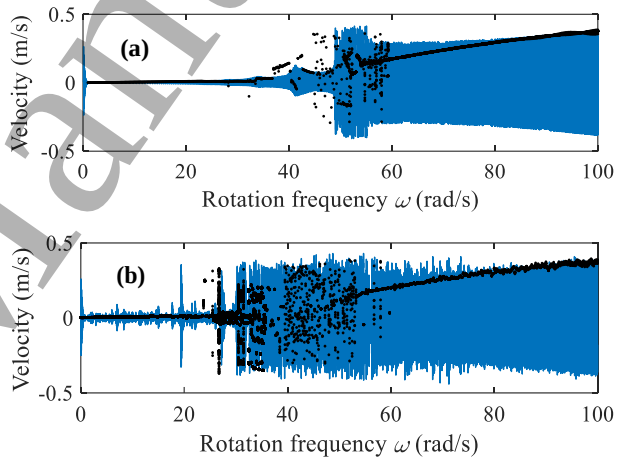


**Figure 5.** Velocity and bifurcation responses of harmonic excitation of rotational gravity under the optimized centrifugal distance of 6.45 cm: (a) without combination of noise excitation and (b) with noise excitation.

Figure 5 demonstrates the velocity as well as bifurcation responses of the system under the optimally centrifugal distance of 6.45 cm. It can be observed that the stabilized phenomenon of stochastic resonance can improve the velocity response up to 50 rad/s by comparing the two conditions with and without a combination of noise excitations. When the rotation frequency exceeds rotation frequency of 50 rad/s, unstable and high-energy orbit motion continues to stabilize the response level. Consequently, in this research, the boundary frequency was determined to be 50 rad/s to verify the positive effect of the optimized centrifugal distance on the performance of rotation-induced energy harvesting

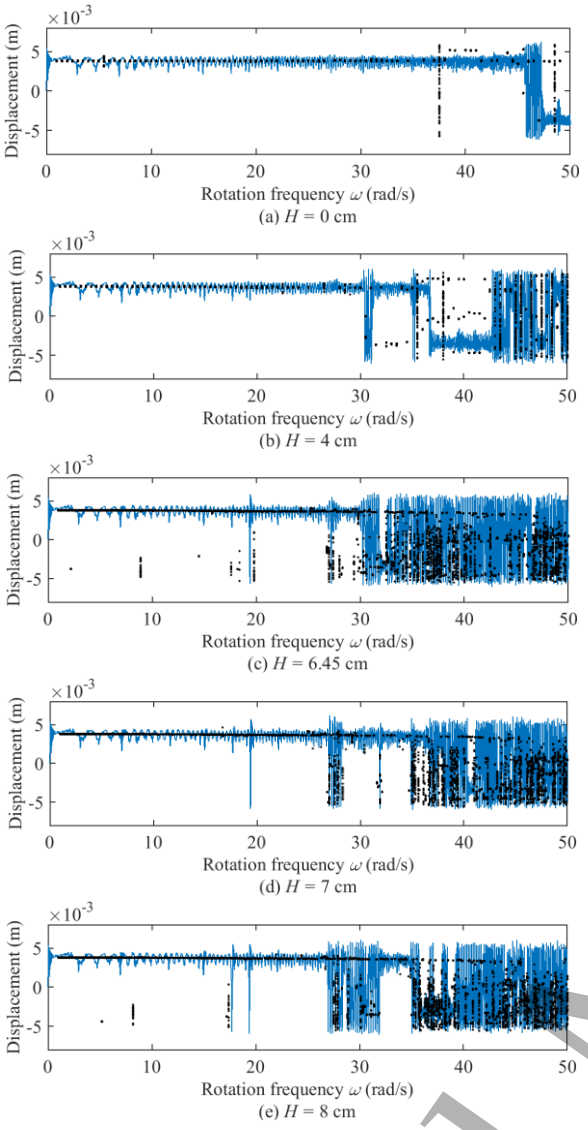


**Figure 6.** Comparison results of displacement and bifurcation responses under different centrifugal distances: (a) 0 cm, (b) 4 cm, (c) 6.45 cm, (d) 7 cm and (e) 8 cm.

Figure 6 shows the comparison results of the bifurcation and displacement responses under different centrifugal distances based on the stiffness-tunable dynamic equation. The different centrifugal distances were set to 0 cm, 4 cm, 6.45 cm, 7 cm and 8 cm. The blue curve reflects the displacement response and the black dotted curve represents the bifurcation response under the sweep frequency range of 0 rad/s–50 rad/s with the same running time of 56 s. As shown in figures 6(a) and 6(b), it can be observed that the piezoelectric cantilever beam mainly fluctuates around one equilibrium potential well at the distance of 0 cm, and the probability of transiting between two potential wells increases as the distance reaches 4 cm. While the centrifugal distance is tuned to the optimally centrifugal distance 6.45 cm derived by theoretical analysis, the beam can be activated to continually oscillate between two equilibrium potential wells over the range of 30 rad/s to 50 rad/s.

As the centrifugal distance increased further, the phenomenon of continuous oscillation was difficult to stabilize in the range of 30 rad/s–50 rad/s, as shown in figures 6(d) and 6(e). Therefore, the simulation results verified that the displacement performance of the tunable stochastic resonance can be optimized when the centrifugal distance reaching 6.45 cm as theoretically calculated shown in figure 3. In addition, the corresponding phase trajectories without consideration of the centrifugal effect and with the optimally centrifugal distance are compared, as shown in figures 7(a) and 7(b). Figure 8(a) demonstrates the simulation results of the amplitude of velocity response corresponding to its optimally matching centrifugal distance of 6.45 cm, it can be observed that the amplitude of velocity begins to increase from 30 rad/s due to the frequency of stochastic resonance approaching to rotating frequency of $\omega$. From figures 8(b) and 8(c), it can be obviously distinguished the larger instantaneous velocity at the matching well frequency than the deviating frequency before frequency of 30 rad/s.

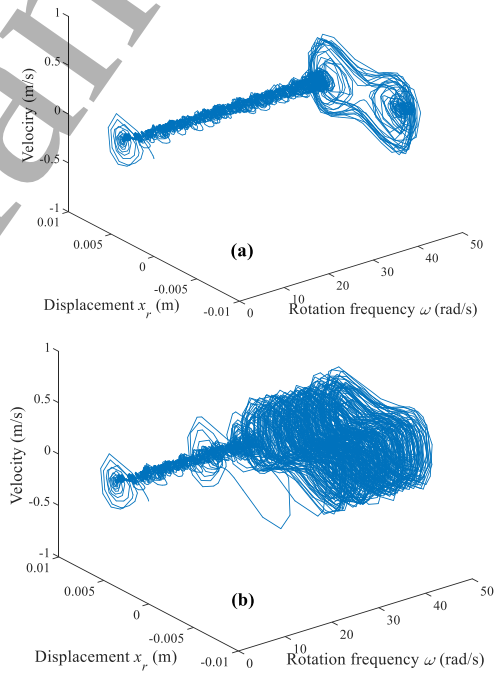


**Figure 7.** Phase trajectories of the response with combination of noise excitation under centrifugal distances: (a) $H$=0 cm and (b) $H$=6.45 cm.

In order to investigate the influence caused by centrifugal effect on energy harvesting capability of nonlinear bistable system, the specifically parametric conditions are determined as $C$=2.95×10$^{-8}$ F, $R_l$=33.4 kΩ, $\theta_p$= − 9.2×10$^{-5}$ N/V. According to equation (14), the voltages produced across the external load resistances $R_l$ can be obtained based on the displacement responses, as shown in figure 8.

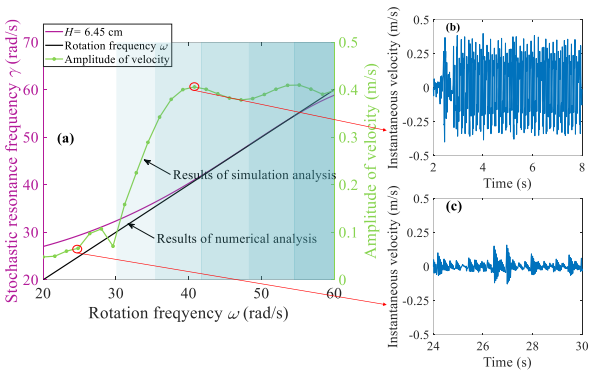


**Figure 8.** The simulation results of the velocity response: (a) under the optimally matching centrifugal distance of 6.45 cm derived from numerical analysis, (b) and (c) its corresponding instantaneous velocities at matching well and deviating frequencies.

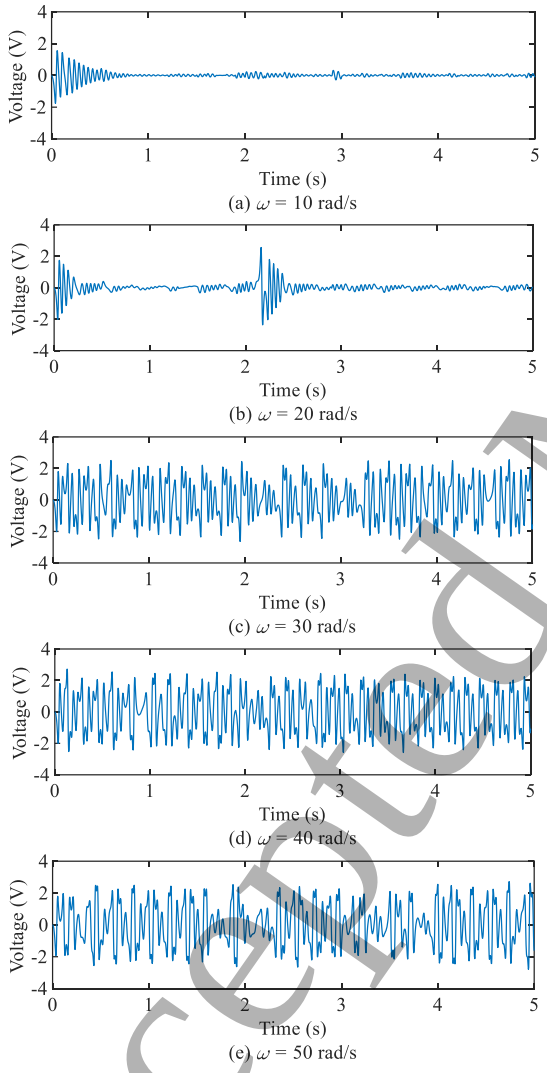


**Figure 9.** Voltages produced across the external load resistances at optimally centrifugal distance under the different harmonic rotation frequencies: (a) 10 rad/s, (b) 20 rad/s, (c) 30 rad/s, (d) 40 rad/s and (e) 50 rad/s.

It can be observed that the fluctuation in almost one potential well causes the produced voltages to maintain a low amplitude level under rotation frequencies of 10 rad/s and 20 rad/s in figures 9(a) and 9(b). As the harmonic frequency increased by 30 rad/s, 40 rad/s and 50 rad/s, as shown in figures 9(a), 9(b) and 9(c), respectively, the voltage amplitudes were significantly improved owing to the good matching relationship between the stochastic resonance and harmonic rotation frequency, as numerically demonstrated in figure 4. Furthermore, figure 10 summarizes the derived simulation results of the RMS value of the voltage produced at different centrifugal distances. It can be revealed that with an increase in the centrifugal distance, the efficient harvesting bandwidth is further enlarged, and the widest bandwidth is found to be up to 6.45 cm, after which, it embodies a trend of gradually decreasing. Therefore, it can be verified that the optimally centrifugal distance derived from the simulation result is consistent with the theoretical solution based on equation (33) and the numerical analysis shown in figure 4.

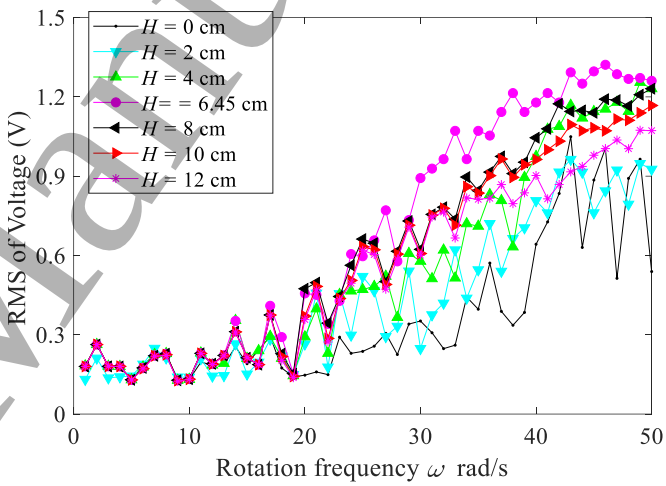


**Figure 10.** The RMS value of the produced voltage at the different centrifugal distances.

## 5. EXPERIMENTAL VALIDATION

Figure 11 demonstrates that an actual validation experiment of rotation combined with vibration was conducted to corroborate the centrifugal distance theoretically optimized under a rotation frequency range of 10 rad/s–50 rad/s. As shown in figure 11(a), the rotation apparatus providing one condition of rotation was driven by a servo motor (SGM7J-04A7C6S, Yaskawa Electric Co., Ltd), Shanghai, China), and a ceramic piezoelectric layer (PZT-5A, Doctor Source Technology Co., Ltd., Guilin, China) was attached to the root of the beam, which was made of aluminum alloy. At the free tip position of the cantilever beam, an Nd-Fe-B magnet with high magnetization strength is bonded, and in the opposite direction, a fixed magnet with the same magnetic polarity

and dimensional size is positioned to generate the nonlinear restoring force of the bistable system. Two high-precision laser displacement sensors (HG-C1100, Panasonic, Ōsaka, Japan) were mounted on the rotating platform to measure the displacement responses of the piezoelectric layer and end magnet. It should be noted that the limitation of the maximum acceleration time to be 10 s of the servo motor using during the experimenting, brings the experimental condition under constant rotation frequencies over the range of 10 rad/s–50 rad/s with the interval of 10 rad/s, for convincing the effectiveness of the responses of displacement and harvested power.

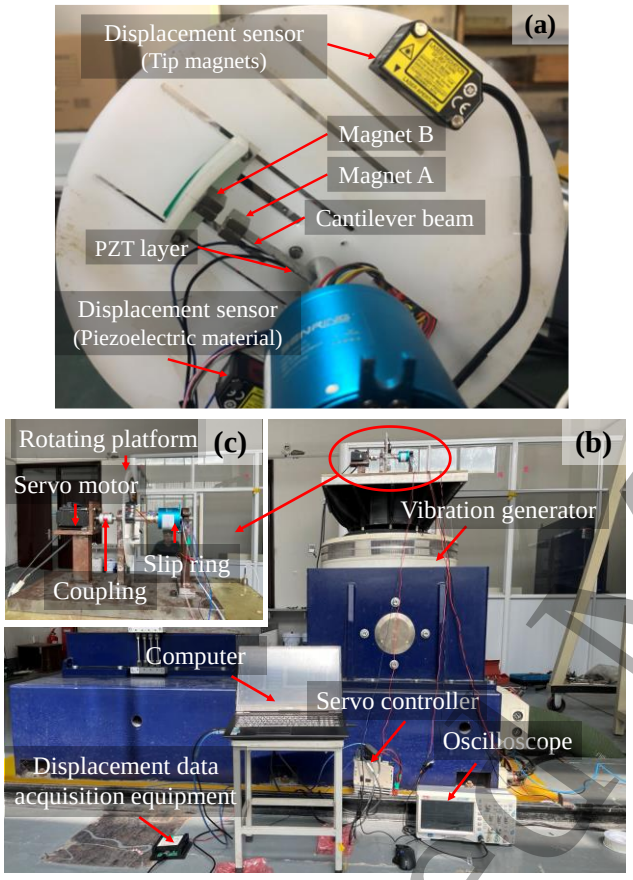


**Figure 11.** Experimental apparatuses for generating the conditions of rotation and vibration: (a) rotation environment, (b) entire equipment by mounted the rotating platform on a vibration generator and (c) specifically components for establishing the rotation environment.

Figure 11(b) shows that the experimental apparatuses was comprised of a rotating platform mounted on a vibration generator (MPA409/LS444M/GT680M, ETS Solutions Co., Ltd., Suzhou, China) driven by a powerful controller board (SGD7S-2R8A, Yaskawa Electric Co., Ltd., Shanghai, China) with Sigma Win+ software used to provide the other condition for generating vibration. The displacement and voltage data were collected through a slip ring (G012-12, SenRing Electronics Co., Ltd, Shenzhen, China) using acquisition equipment and a high-speed oscilloscope (UPO2000CS, Uni-trend Technology Co., Ltd., Guangzhou, China), as shown in figures 11(b) and 11(c).

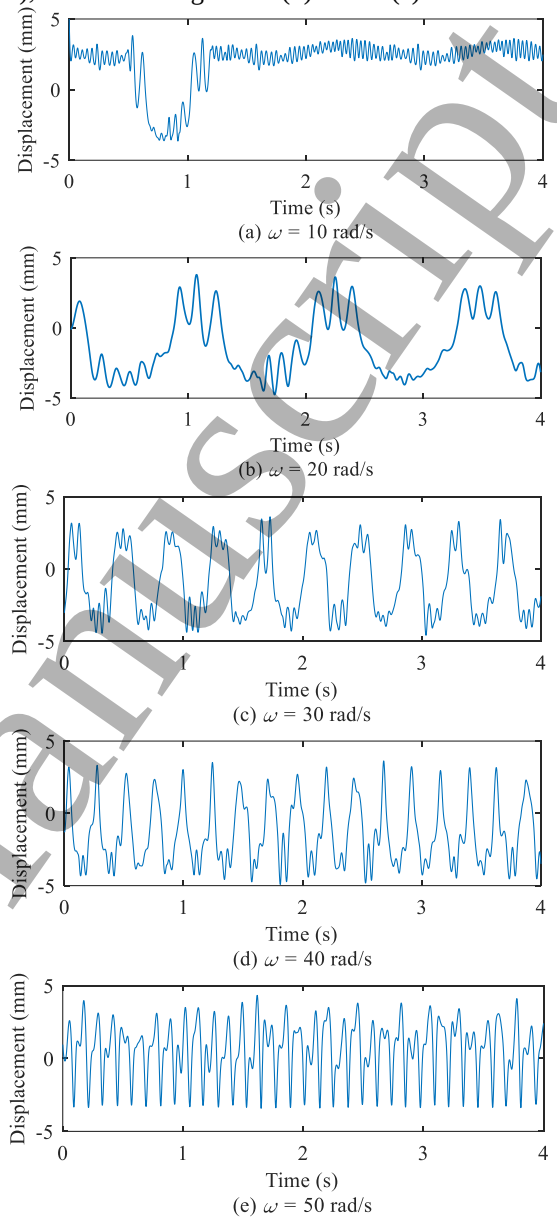


**Figure 12.** Comparison of experimental results regarding the instantaneous displacement at optimally centrifugal distance of 6.45 cm under the different harmonic rotation frequencies: (a) 10 rad/s, (b) 20 rad/s, (c) 30 rad/s, (d) 40 rad/s and (e) 50 rad/s, which corresponds to the points as highlighted in figure 4.

Figure 12 shows an experimental comparison of the instantaneous displacements at different harmonic rotation frequencies corresponding to the points as highlighted in figure 4, and the maximum rotation frequency was determined to be the 50 rad/s based on the boundary frequency as numerically derived from figure 5. It can be demonstrated that the cantilever almost fluctuates around

one potential well, causing a low amplitude level under rotation frequencies of 10 rad/s and 20 rad/s, as shown in figures 12(a) and 12(b). As the harmonic frequency exceeds 30 rad/s, as shown in figures 12(a), 12(b) and 12(c), the displacement amplitudes are significantly improved because of the occurrence of tunable stochastic resonance, as results of sweep simulation shown in figure 6(c).

Moreover, figure 13 gives the corresponding phase trajectories of the displacement response under different harmonic rotation frequencies, which reflect the responses possessing the typical characteristics of transition waiting behavior for the phenomenon of stochastic resonance. Furthermore, the voltages produced across the external load resistances $R_l$ can be obtained, as shown in figure 14, and the instantaneous voltage can be continually delivered with a maximum amplitude of 2 V, due to the well-matched relationship between stochastic resonance and harmonic rotation frequency, as demonstrated in figure 9.

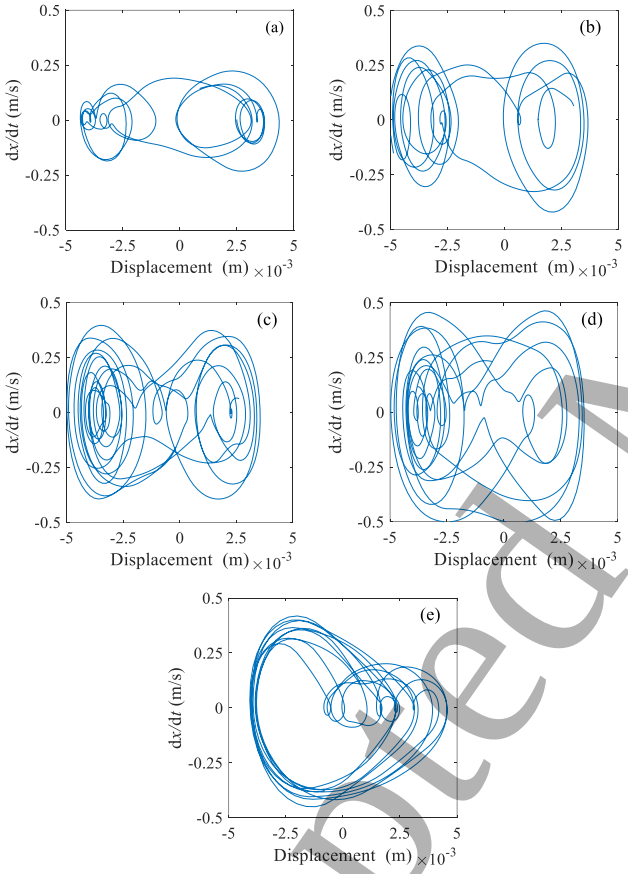


**Figure 13.** The corresponding phase trajectories of the displacement response under the different harmonic rotation frequencies: (a) 10 rad/s, (b) 20 rad/s, (c) 30 rad/s, (d) 40 rad/s and (e) 50 rad/s.

Furthermore, the results laboratory experiment as well as simulation based on equations (14) and (15) simultaneously validated that the centrifugal distance is tuned to be that of the optimal 6.45 cm as theoretically derived, and the effective bandwidth of energy harvesting can be stabilized from 30 rad/s to 50 rad/s. Its RMS voltage can reach a value of 1.23 V corresponding to a harvesting average power of 45.55 μW, owing to the hight matching relationship between stochastic resonance and external rotation frequencies, as shown in figure 15.

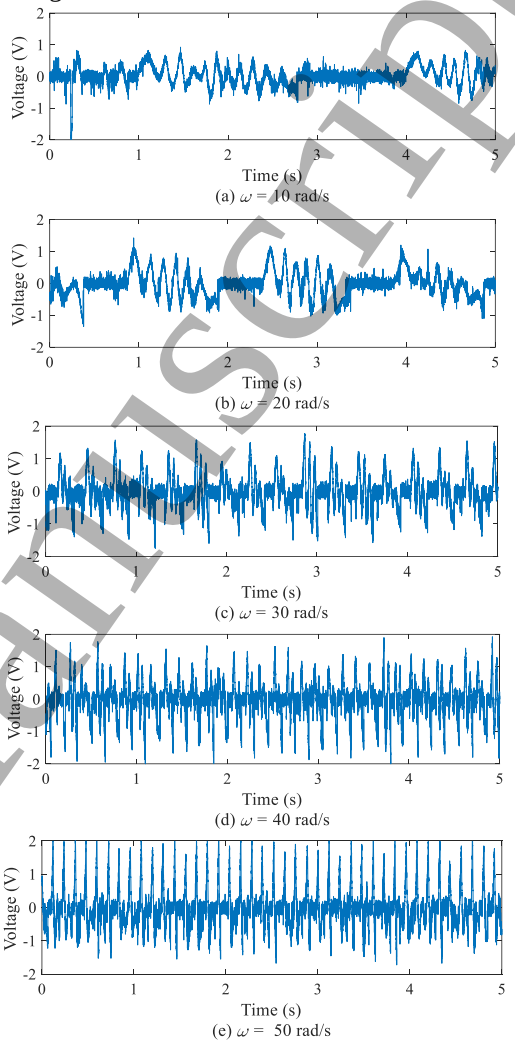


**Figure 14.** Comparison of experimental results regarding the instantaneous voltage at optimally centrifugal distance of 6.45 cm under the different harmonic rotation frequencies: (a) 10 rad/s, (b) 20 rad/s, (c) 30 rad/s, (d) 40 rad/s and (e) 50 rad/s.

Finally, the RMS of the voltage across the external load resistance $R_l$ was compared under different centrifugal distances of 0 cm, 4 cm, 6.45 cm and 8 cm. As shown in figure 16, when the centrifugal distance $H$ is 0 cm, the RMS of voltage increases slowly with maximum RMS value of 0.78 V within the rotation frequency range of 50 rad/s. Nevertheless, as the centrifugal distance is tuned to an optimal value of 6.45 cm, the best performance is clearly revealed in the range of 30–50 rad/s among the different centrifugal distances, with a maximum voltage of 1.23 V.

Consequently, it can be validated that the experimental results are in good agreement with the theoretical analysis as well as simulation results based on optimization of tunable stochastic resonance as obtained from equation (33) and figure 10.

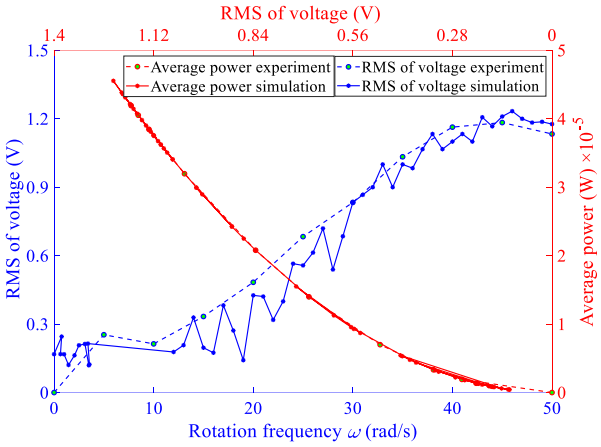


**Figure 15.** Comparisons of experimental with simulation results regarding average power and the RMS value of the output voltage, across the external load resistances $R_l$ at the optimally centrifugal distance of 6.45 cm.

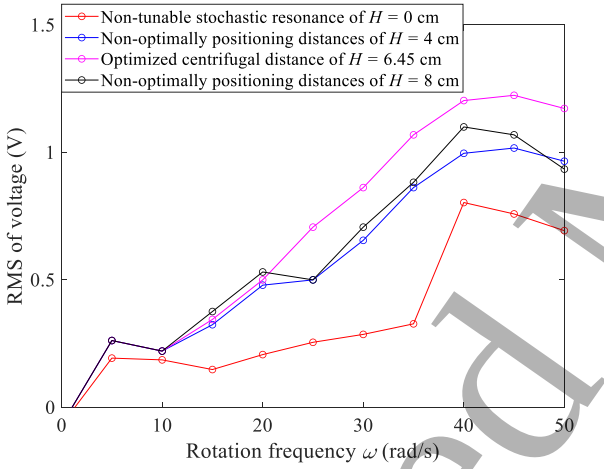


**Figure 16.** Comparison of RMS of voltages under different centrifugal distances of non-tunable stochastic resonance of 0 cm, non-optimally positioning distances of 4 cm, optimized centrifugal distance of 6.45 cm and non-optimally positioning distances of 8 cm.

## 6. CONCLUSION

In this study, a principle for optimizing the centrifugal distance was theoretically proposed instead of the previous means of physically parametric adjustment, for the application of rotation-induced energy harvesting. It can minimize the negative effect of low-energy orbit, owing to the optimally stabilized stochastic resonance, particularly over the relatively low-frequency range before high-energy orbit oscillation. Based on the established coupling dynamic equation with stiffness tunable characteristics, the optimum centrifugal distance is theoretically solved by the frequency matching relationship between the Kramers escape rate and the externally rotating environment. The results of simulations indicated that the optimized centrifugal distance of 6.45 cm as theoretically derived, can effectively improve the bandwidth for energy harvesting when compared with different centrifugal distances. Furthermore, the experimental results revealed that the effective bandwidth of energy harvesting can be stabilized from 30 rad/s to 50 rad/s. Its maximum root mean square (RMS) voltage can reach the value of 1.23 V corresponding to a harvesting average power of 45.55 μW, owing to the high matching relationship between stochastic resonance and external rotation frequencies. Consequently, it was concluded that the optimization of the theoretical principle can significantly contribute to the understanding of the relationship between the centrifugal effect and rotating environments, to facilitate the potential applicability of stochastic resonance in various applications such as vehicle tires, mechanical gears and shafts. This can be further suggested that the coordinately combing of tunable stochastic resonance and different inter-well oscillations would be a promising means for comprehensively improving the overall bandwidth for rotational energy harvesting.

## ACKNOWLEDGEMENTS

The authors acknowledge funding support from the Post-doctoral Research Foundation of China (Grant No. 2020M681497), the Youth Talent Cultivation Program of Jiangsu University, and the project funded by the National Natural Science Foundation of China (Grant No. 12172153).

## Data Availability Statements

The authors declare that the data supporting the findings of this study are available within the article.

## REFERENCES

[1] Li Z 2019 Manufacture, assembly, test and analysis of button cell *Modern Industrial Economy and Information Technology* **9** 19–20

[2] Oudenhoven J F M, Vullers R J M and Van Schaijk R 2012. A review of the present situation and future developments of micro-batteries for wireless autonomous sensor systems *International Journal of Energy Research* **36** 1139–50

[3] Löhndorf M, Kvisterøy T, Westby E and Halvorsen E 2007 Evaluation of energy harvesting concepts for tire pressure monitoring systems *Proceedings of Power MEMS* pp. 331–34

[4] Kubba A E and Jiang K 2014 A comprehensive study on technologies of tyre monitoring systems and possible energy solutions *Sensors* **14** 10306–345
[5] Eshghi A T, Lee S, Sadoughi M K, Hu C, Kim Y C and Seo J H 2017 Design optimization under uncertainty and speed variability for a piezoelectric energy harvester powering a tire pressure monitoring sensor *Smart Materials and Structures* **26** 105037
[6] Wang Z L, Chen J and Lin L 2015 Progress in triboelectric nanogenerators as a new energy technology and self-powered sensors *Energy & Environmental Science* **8** 2250–82
[7] Salehi H, Burgueño R, Chakrabartty S, Lajnef N and Alavi A H 2021 A comprehensive review of self-powered sensors in civil infrastructure: State-of-the-art and future research trends *Engineering Structures* **234** 111963
[8] Glynne-Jones P and White N M 2001 Self‐powered systems: a review of energy sources *Sensor Review* **21** 91–97
[9] Safaei M, Sodano H A and Anton S R 2019 A review of energy harvesting using piezoelectric materials: state-of-the-art a decade later (2008–2018) *Smart Materials and Structures* **28** 113001
[10] Beeby S P, Wang L, Zhu D, Weddell A S, Merrett G V, Stark B, Szarka G and Al-Hashimi B M 2013 A comparison of power output from linear and nonlinear kinetic energy harvesters using real vibration data *Smart Materials and Structures* **22** 075022
[11] Kim H S, Kim J H and Kim J 2011 A review of piezoelectric energy harvesting based on vibration *International Journal of Precision Engineering and Manufacturing* **12** 1129–41
[12] Kundu S and Nemade H B 2016 Modeling and simulation of a piezoelectric vibration energy harvester *Procedia Engineering* **144** 568–75
[13] Zhou S, Cao J, Wang W, Liu S and Lin J 2015 Modeling and experimental verification of doubly nonlinear magnet-coupled piezoelectric energy harvesting from ambient vibration *Smart Materials and Structures* **24** 055008
[14] Wang W, Cao J, Bowen C R and Litak G 2019 Probability and output analysis of asymmetric bistable energy harvesters subjected to Gaussian white noise. *The European Physical Journal Plus* **134** 558
[15] Lu Z Q, Zhang F Y, Fu H L, Ding H and Chen L Q 2021 Rotational nonlinear double-beam energy harvesting *Smart Materials and Structures* **31** 025020
[16] Vijayan K, Friswell M I, Khodaparast H H and Adhikari S 2015 Non-linear energy harvesting from coupled impacting beams *International Journal of Mechanical Sciences* **96** 101–09
[17] Mantegna R N, Spagnolo B and Trapanese M 2000 Linear and nonlinear experimental regimes of stochastic resonance *Physical Review E* **63** 011101
[18] Agudov N V, Krichigin A V, Valenti D and Spagnolo B 2010 Stochastic resonance in a trapping overdamped monostable system *Physical Review E* **81** 051123
[19] Chouhan R, Jha R K and Biswas P K 2013 Enhancement of dark and low-contrast images using dynamic stochastic resonance *IET Image Processing* **7** 174–84
[20] Danziger Z and Grill W M 2015 A neuron model of stochastic resonance using rectangular pulse trains *Journal of Computational Neuroscience* **38** 53–66
[21] Kramers H A 1940 Brownian motion in a field of force and the diffusion model of chemical reactions *Physica* **7** 284–304
[22] McNamara B and Wiesenfeld K 1989 Theory of stochastic resonance *Physical review A* **39** 4854
[23] Hänggi P Talkner P and Borkovec M 1990 Reaction-rate theory: fifty years after Kramers *Reviews of modern physics* **62** 251
[24] McInnes C R, Gorman D G and Cartmell M P 2008 Enhanced vibrational energy harvesting using nonlinear stochastic resonance *Journal of Sound and Vibration* **318** 655–662
[25] Li H, Qin W, Deng W and Tian R 2016 Improving energy harvesting by stochastic resonance in a laminated bistable beam *The European Physical Journal Plus* **131** 1–9
[26] Zheng R, Nakano K, Hu H, Su D and Cartmell M P 2014 An application of stochastic resonance for energy harvesting in a bistable vibrating system *Journal of Sound and Vibration* **333** 2568–587
[27] Leng Y and Lai Z 2014 Generalized parametric stochastic resonance of duffing oscillator based on Kramers escape rate *Acta Physica Sinica* **63** 38–46
[28] Zhang Y, Zheng R, Kaizuka T, Su D, Nakano K and Cartmell M P 2015 Broadband vibration energy harvesting by application of stochastic resonance from rotational environments *The European Physical Journal Special Topics* **224** 2687–701
[29] Zhang Y, Zheng R, Shimono K, Kaizuka T and Nakano K 2016 Effectiveness testing of a piezoelectric energy harvester for an automobile wheel using stochastic resonance *Sensors* **16** 1727
[30] Zhang Y, Cai Y, Teng X, Zheng R and Nakano K 2020 Combining sustainable stochastic resonance with high-energy orbit oscillation to broaden rotational bandwidth of energy harvesting from tire *AIP Advances* **10** 015011
[31] Kim H, Tai W C, Zhou S and Zuo L 2017 Stochastic resonance energy harvesting for a rotating shaft subject to random and periodic vibrations: influence of

potential function asymmetry and frequency sweep *Smart Materials and Structures* **26** 115011

[32] Kim H, Tai W C, Parker J and Zuo L 2019 Self-tuning stochastic resonance energy harvesting for rotating systems under modulated noise and its application to smart tires *Mechanical Systems and Signal Processing* **122** 769–85

[33] Fu H and Yeatman E M 2019 Rotational energy harvesting using bi-stability and frequency up-conversion for low-power sensing applications: Theoretical modelling and experimental validation *Mechanical Systems and Signal Processing* **125** 229–244

[34] Zhao L, Zou H, Gao Q, Yan G, Wu Z, Liu F, Wei K, Yang B and Zhang W 2020 Design, modeling and experimental investigation of a magnetically modulated rotational energy harvester for low frequency and irregular vibration Science *China Technological Sciences* **63** 2051–2062

[35] Zhao L, Zou H X, Wu Z Y, Gao Q H, Yan G, Liu F R, Wei K X and Zhang W M 2022 Dynamically synergistic regulation mechanism for rotation energy harvesting *Mechanical Systems and Signal Processing* **169** 108637

[36] Fang S, Wang S, Zhou S, Yang Z and Liao W H 2020 Exploiting the advantages of the centrifugal softening effect in rotational impact energy harvesting *Applied Physics Letters* **116** 063903

[37] Fang, S, Wang S, Zhou S, Yang Z and Liao W H 2020 Analytical and experimental investigation of the centrifugal softening and stiffening effects in rotational energy harvesting *Journal of Sound and Vibration* **488** 115643

[38] Mei X, Zhou S, Yang Z, Kaizuka T and Nakano K 2020 A tri-stable energy harvester in rotational motion: Modeling, theoretical analyses and experiments *Journal of Sound and Vibration* **469** 115142

[39] Mei X, Zhou S, Yang Z, Kaizuka T and Nakano K 2021 Enhancing energy harvesting in low-frequency rotational motion by a quad-stable energy harvester with time-varying potential wells *Mechanical Systems and Signal Processing* **148** 107167

[40] Ma X, Li H, Zhou S, Yang Z and Litak G 2022 Characterizing nonlinear characteristics of asymmetric tristable energy harvesters *Mechanical Systems and Signal Processing* **168** 108612

[41] Sun S and Cao S 2012 Dynamic modeling and analysis of bistable piezoelectric cantilever power generation system *Acta Physica Sinica* **61** 95–106

[42] Zhang Y, Nakano K, Zheng R and Cartmell M P 2016 Adjustable nonlinear mechanism system for wideband energy harvesting in rotational circumstances *Journal of Physics: Conference Series* **744** 012079

[43] Zhang Y, Zheng R, Nakano K and Cartmell M P 2018 Stabilising high energy orbit oscillations by the utilisation of centrifugal effects for rotating-tyre-induced energy harvesting Applied Physics Letters 112 143901

[44] Lefeuvre E, Badel A, Richard C, Petit L and Guyomar D 2006 A comparison between several vibration-powered piezoelectric generators for standalone systems Sensors and Actuators A: Physical 126 405–416

[45] Gammaitoni L, Neri I and Vocca H 2009 Nonlinear oscillators for vibration energy harvesting Applied Physics Letters 16 164102

[46] Stanton S C, McGehee C C and Mann B P 2009 Reversible hysteresis for broadband magnetopiezoelastic energy harvesting Applied Physics Letters 95 174103

[47] Priya S and Inman D J 2009 Energy harvesting technologies (New York, PA: Springer)

[48] Daqaq M F, Masana R, Erturk A and Quinn D D 2014 On the role of nonlinearities in vibratory energy harvesting: a critical review and discussion Applied Mechanics Reviews 66 040801–1

[49] Zhang Y, Zhao X and Wang W 2021 Rotation-induced-tunable stochastic resonance for stabilizing sustainability of energy harvesting. In 2021 IEEE 20th International Conference on Micro and Nanotechnology for Power Generation and Energy *Conversion Applications (PowerMEMS)* (Exeter)